Vibrationally hot emission and electronic relaxation of CO in Ne matrix

Johannes Bahrdt and Nikolaus Schwentner

Citation: The Journal of Chemical Physics **88**, 2869 (1988); doi: 10.1063/1.453979
View online: http://dx.doi.org/10.1063/1.453979
View Table of Contents: http://scitation.aip.org/content/aip/journal/jcp/88/5?ver=pdfcov
Published by the AIP Publishing

Vibrationally hot emission and electronic relaxation of CO in Ne matrix

Johannes Bahrdt and Nikolaus Schwentner
Institut für Atom- und Festkörperphysik, Arnimallee 14 D-1000 Berlin 33, Federal Republic of Germany

(Received 14 September 1987; accepted 27 October 1987)

Vibrational progressions due to radiative decay of $A\ ^1\Pi$ ($v' = 0, 2, 3\ 5, 6, 8$), $e\ ^3\Sigma$ ($v' = 0, 3, 5, 12$), $a'\ ^3\Sigma$ ($v' = 5, 14$), $d\ ^3\Delta$ ($v' = 3, 5$), $a\ ^3\Pi$ ($v' = 0, 1, 2$) to the ground state and of $e\ ^3\Sigma$ ($v' = 3, 5, 7, 9, 11, 12$) and $d\ ^3\Delta$ ($v' = 3, 7, 11$) to the $a\ ^3\Pi$ state have been observed for selective excitation of $A\ ^1\Pi$ ($v' = 0, \ldots, 8$). The intersystem crossing rate constants, the bottle necks, pathways and rate constants for internal conversion in the triplet levels and the triplet–singlet radiative rate constants are explained by an intramolecular mixing of electronic states and electron–phonon coupling with the matrix.

I. INTRODUCTION

Energy dissipation in electronically and vibrationally excited states in the condensed phase is in general fast. Therefore it is difficult to disentangle experimentally the complex interplay of different relaxation processes. Electronic and vibrational states of molecules in solid matrices can serve as probes to study the energy dissipation into localized and lattice modes. It is now well-documented[1,2] that the rate constants for electronic and vibrational relaxation of diatomic molecules in rare gas matrices cover a range from 10^{12} up to 1 s^{-1}. There has been some emphasis in the last years in the investigation of larger molecules with higher level densities to follow the competition of different internal and external modes.[3] But still several conceptual questions have to be answered even for the simpler cases of diatomic molecules. For hydrides a conversion into rotational and librational modes seems to be dominant.[4] The accepting modes for nonhydride diatomics are less clear. There is a beautiful study of stepwise internal conversion for CN[5] in a rare gas matrix which has been attributed finally to rotational excitations[6] and which should be seen in connection with recent state to state collisional induced relaxation studies in the gas phase.[7] For $(O_2)_2$[8] it has also been shown that intersystem crossing is fast enough to compete with vibrational relaxation in favorable cases. In As_2[9] on the other hand, internal conversion in triplet states and intersystem crossing to the ground state is slow. In addition, in the $A\ ^3\Sigma_u$ state of N_2 vibrational relaxation is also extremely slow,[10,11] leading Xe matrices to relaxation only by intermolecular energy transfer to quite remote neighbors.[11] Vibrationally hot emission has been reported besides N_2[10–12] also from the $B\ ^2\Pi$ valence state of NO and even from the $A\ ^2\Sigma^+$ Rydberg state of NO.[13] More systematic studies seem to be necessary to derive a general quantitative model for the competition of intersystem crossing, internal conversion and vibrational relaxation.

This work considers primarily contributions to the relaxation processes by mixing of electronic states[14,15] and the relation to gas-phase collision processes. The $A\ ^1\Pi$ state of CO is embedded in a manifold of triplet states[16] and is a good candidate for a case study. The spectroscopic constants and the interaction matrix elements are well-known from high resolution gas phase data[17] and reversible intersystem crossing induced by collision with rare gases has been investigated in detail.[18] High resolution absorption spectra have been reported for the $A\ ^1\Pi$ and several triplet states of CO in Xe, Kr, and Ar matrices[19] but only for the $A\ ^1\Pi$ state in Ne matrix.[20,21] Until now only emission from the vibrationally relaxed lowest triplet state $a\ ^3\Pi$ has been observed in Ne, Ar, and Kr matrices.[19] In this paper emissions from several vibrationally hot triplet states and the vibrationally hot $A\ ^1\Pi$ singlet state of CO in Ne matrix will be presented which provide for the first time insight into the relaxation processes. The time resolved data indicate that the population rests in specific bottlenecks for 10^{-8} to 10^{-4} s, and from the intensities intersystem crossing rate constants in the 10^{-11} s range are derived. It has to be pointed out that CO in Ne according to these data is a rare example showing vibrational hot emission up to $v' = 12$ and from five different nested electronic states of singlet and triplet character. A relaxation cascade is constructed for the selective excitation of $A\ ^1\Pi$ ($v' = 0, \ldots, 8$) vibrational levels.

The radiationless relaxation processes are attributed to a mixing of electronic states similar to the gas phase[14,18] but modified to include the electron–phonon coupling in the matrix. The rate constants are determined by an intramolecular electronic coupling matrix element, an intramolecular Franck–Condon factor, both known from the gas phase, a CO-matrix Franck–Condon factor known from spectroscopic data, and a phonon relaxation rate in the final state. In the discussion these parameter-free rate constants are confronted with the experimental relaxation cascade, with special emphasis on a depopulation and repopulation of $A\ ^1\Pi$ vibrational levels by reversible intersystem crossing on a 10^{-11} s time scale and on vibrational relaxation by internal conversion in the triplet manifold. The coherent mixing of the singlet and triplet states should also explain the observed shortening of the radiative lifetimes in triplet–singlet transitions in a consistent way. Furthermore evidence for a multiphonon (or libron) vibrational relaxation in the $v' = 1, 2$ levels of the $a\ ^3\Pi$ state on a 10^{-4} s time scale will be given.

II. EXPERIMENTAL SETUP

The vibrational levels $v' = 0$–8 of the $A\ ^1\Pi$ state have been excited selectively by monochromatrized Synchrotron radiation and emission spectra have been recorded in the spectral range from 140 up to 800 nm. For several selected

 0021-9606/88/052869-15$02.10

emission bands also the dependence of the intensity in the emission band on the excitation wavelength, i.e., on the initially populated level has been measured. These spectra are called excitation spectra. Furthermore the time course of the intensity in a specific emission band for a selectively excited intial level has been recorded by exploiting the pulse structure of Synchrotron radiation. The experiments have been performed at the beam line 3 m Nim II at the storage ring BESSY in Berlin[19] and also at the beam line SUPERLUMI at the storage ring DORIS in Hamburg.[22,23] Both beam lines are optimized for a high flux and high resolution for the exciting light in the spectral range 30–300 nm and for a high detection efficiency for the emitted light in the range from 50–1000 nm. In both beam lines about 50 mrad of the horizontal cone of a bending magnet are focused by two mirrors into the entrance slit of a primary monochromator which provides an ultimate resolution of about 0.005 nm (BESSY) or 0.007 nm (DORIS). The dispersed light is focused onto the sample by a further mirror. The light spot at the sample serves as an entrance slit for two independent monochromators for the emitted light. One covers the spectral range from 50–300 nm and the other one the range from 200–1000 nm both with a typical resolution of 1 nm. For further details see Refs. 19, 22, and 23. The emission spectra in the range from 300–800 nm have been taken at the BESSY beam line with a RCA C31034A detector. The time resolved experiments require a time interval between two successive pulses which is at least of the order of the time constants to be measured. The time resolved experiments have been performed therefore at the storage ring DORIS which has a typical pulse length of 0.3 ns and a pulse spacing in the single bunch mode of 960 ns. Single photon counting by a Valvo XP 2020 (300–800 nm) and a Hamamatsu 1460 solar blind detector (140–200 nm), and standard time to amplitude conversion[24] have been applied in the time resolved experiments. A time resolution of 0.8 ns has been achieved which has been tested by the prompt stray light. The excitation spectra for the visible emission bands and the emission spectra in the range 140–300 nm have also been taken at the DORIS beam line.

Ne and CO gases from Linde with purities of 99.999% and 99.99% have been mixed in an ultrahigh vacuum chamber with partial pressures corresponding to the concentrations of the samples. The gases have been condensed on a LiF substrate cooled by a liquid He flow cryostat. The absorption and emission spectra showed no indication for any contamination by for example N_2, O_2, or H_2O. The spectra have been taken at the lowest achieved temperatures of about 8 K. Temperature effects have not been investigated. The CO concentrations have been varied between 0.1 and 2 at. % and no significant changes in the emission spectra have been observed. Therefore we assume that the spectra are representative for well-isolated CO molecules and that interactions between CO molecules are not responsible for the processes discussed in this paper.

III. EXPERIMENTAL RESULTS

Emission bands following the excitation of the vibrational levels $v' = 0$ up to 8 of the $A\ ^1\Pi$ state will be presented. Two classes of emission bands are observed which are illustrated in Fig. 1. One class corresponds to transitions from the vibrationally excited triplet states $e\ ^3\Sigma^-$ and $d\ ^3\Delta$ to the vibrational levels 0–4 of the lowest triplet state $a\ ^3\Pi$. These transitions cover the wavelength range from about 350 nm up to the infrared. The spectra and the corresponding time courses are treated in Sec. III A. The second class (Fig. 1) represents vibrationally hot transitions from the $e\ ^3\Sigma^-$, $d\ ^3\Delta$, $a'\ ^3\Sigma^+$ triplet states and also from the initially excited $A^1\Pi$ singlet state to the singlet ground state $X\ ^1\Sigma_g^+$. The Cameron bands, i.e., transitions from the levels $v' = 0,1,2$ of the $a\ ^3\Pi$ state to the $X\ ^1\Sigma_g^+$ ground state are included in this class. The progressions start at about 130 nm and extend up to 250 nm. The spectra and the decay times are presented in Sec. III B. Finally the intensities in excitation spectra and the fine structure in the $A\ ^1\Pi$ excitation bands due to different sites and due to phonon sidebands will be shown in Sec. III C. In this section the differences in the decay times for excitation into bands of different sites will also be illustrated.

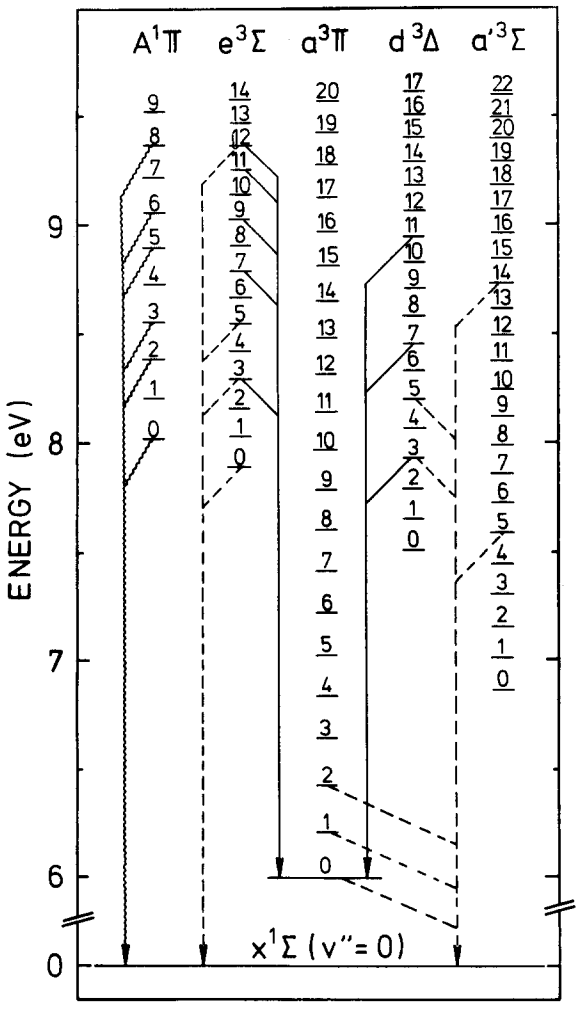

FIG. 1. Energy level scheme of CO indicating the observed radiative transitions in Ne matrix from $A\ ^1\Pi$ (wavy arrows) $e\ ^3\Sigma$, $d\ ^3\Delta$, $a'^3\Sigma$, and $a\ ^3\Pi$ (dashed arrows) to the ground state $X\ ^1\Sigma$ and from $e\ ^3\Sigma$, $d\ ^3\Delta$ (solid arrows) to the $a\ ^3\Pi(v' = 0, 1, 2)$ levels.

A. Emission bands from 350–700 nm

Excitation of A (0 and 1) results only in one very weak emission at 650 nm close to our limit of detection at 700 nm.

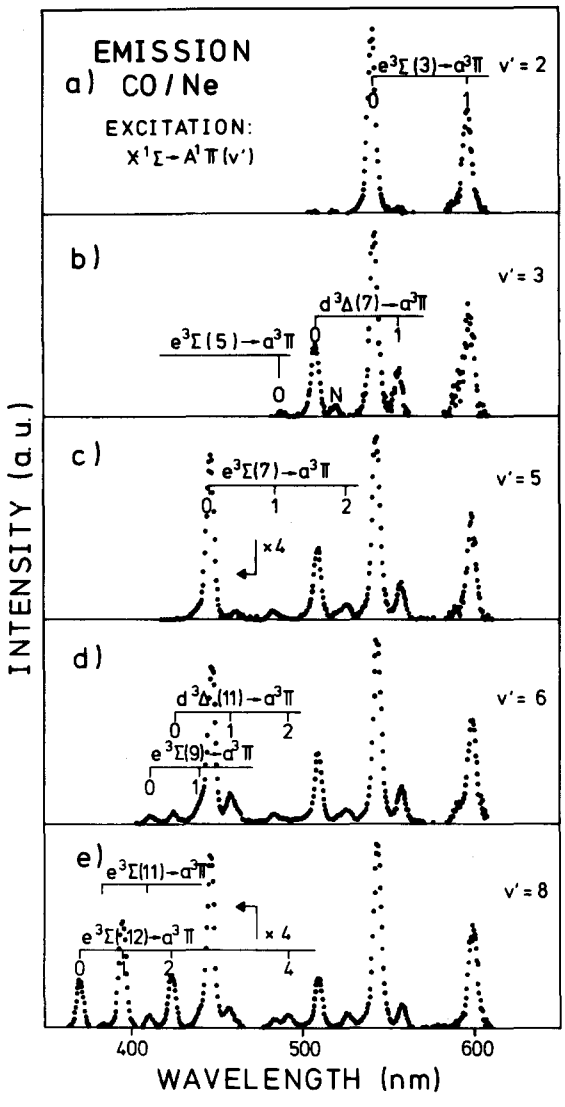

FIG. 2. Emission spectra due to triplet–triplet transitions from $e\,^3\Sigma$ and $d\,^3\Delta$ to $a\,^3\Pi$ corrected for the wavelength dependence of the detection system. The $d(3)\rightarrow a(0)$ band at 650 nm has been omitted. (a) to (e) corresponds to excitation of $v' = 2$, 3, 5, 6, and 8 of $A\,^1\Pi$ respectively.

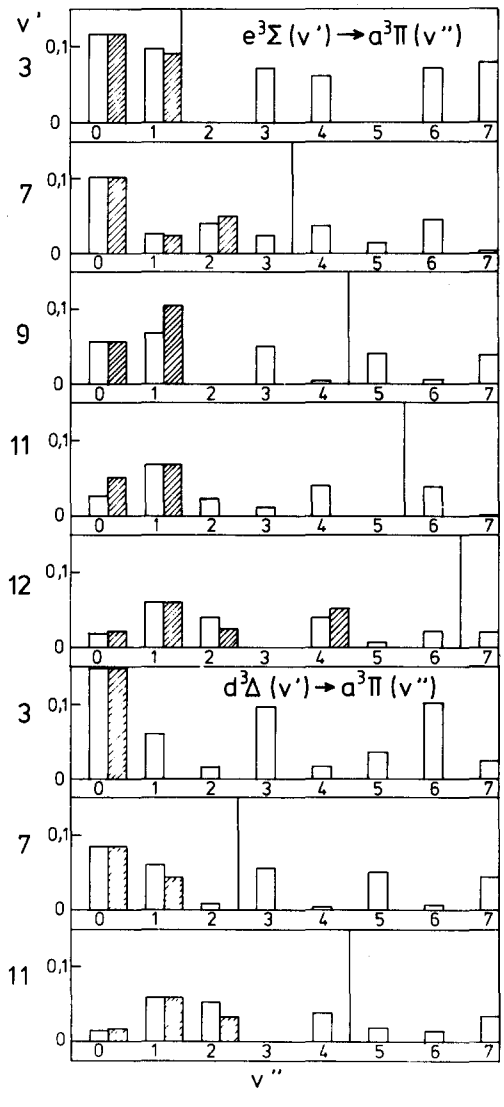

FIG. 3. Franck–Condon factors (open bars) are compared with the emission intensities multiplied by λ^3 (dashed bars) from Fig. 2 for progressions starting from $v' = 3$, 7, 9, 11, 12 of $e\,^3\Sigma$ and $v' = 3$, 7, 11 of $d\,^3\Delta$ and terminating at different v'' levels of $a\,^3\Pi$. The vertical lines indicate the long wavelength detection limit.

It is attributed to a $d(3)\rightarrow a(0)$ transition. The transition energy and the appearance for $A(0)$ allow only a choice for the initial state between $d(3)$, $e(0$ or $1)$, and $a'(8)$ and there is no other choice for the final state. The experience that the matrix shift for valence transitions is in general very small favors an assignment to $d(3)$.

This assignment is strengthened further by the consistency with transition energies of the other emission progressions for which the assignement has been checked by the Franck–Condon factors. Excitation of $A(2)$ leads to two new bands (Fig. 2) in addition to the previous $d(3)$ band. The two bands belong to a $e(3)\rightarrow a(0,1)$ progression according to the criteria given above. Two further bands appear for excitation of $v' = 3$ and $v' = 4$ which are attributed to a $d(7)\rightarrow a(0, 1)$ progression (Fig. 2). An additional $e(7)\rightarrow a(0, 1, 2)$ progression is observed for excitation of $v' = 5$. Two new progressions, $d(11)\rightarrow a(0, 1, 2)$ and $e(9)\rightarrow a(0, 1)$ show up for excitation of $A(6)$ and $A(7)$. Finally excitation of $A\,^1\Pi$ $(v' = 8)$ enlarges the spectrum by the $e(11)\rightarrow a(0, 1)$ and $e(12)\rightarrow a(0, 1, 2, 4)$ progression (Fig. 2). The overview on the spectra in Fig. 2 underlines that increasing the excitation energy causes in general new emission bands from higher energetic triplet states and the previous emission bands from the lower energetic triplet states remain without any significant changes in the relative intensity distributions. The assignments are essentially based on the transition energies which are all close to the gas phase values. In addition the Franck–Condon factors have been calculated using the formalism of Numerov[25] and Cooley[26] and the gas phase Morse potential parameters.[16] The histograms in Fig. 3 compare the calculated Franck–Condon factors divided by λ^3 with the experimental emission bands. In most progressions two, three, or even four bands are sufficiently strong and in all cases the agreement lies within the accuracy of the experimental data. The information in the spectra of Fig. 2 is collected in Fig. 1 and Table I. For excitation of any one of the $A\,^1\Pi$ vibrational levels emission from all those vibrational levels of the $e\,^3\Sigma$ and $d\,^3\Delta$ state to the $a\,^3\Pi$ state have been observed which are marked

TABLE I. Observed long wavelength emission bands (in nm) for CO in Ne with the red shift in meV compared to the gas phase in brackets.

	$v'\backslash v''$	0	1	2	4
$e\,^3\Sigma$	3	543.3(7)	598.9(6)		
	5	488.6(6)			
	7	445.8(7)	483.6(12)	526.0(10)	
	9	411.4(11)			
	11	382.8(13)	409.5(11)		
	12	370.3(13)	395.1(11)	423.7(13)	491.6(11)
	15		359.5(14)		
	16		349.1(13)		
$d\,^3\Delta$	3	648.8(16)			
	7	509.0(17)	557.5(16)		
	11	423.7(15)	457.1(16)	496.0(21)	

by a straight arrow and which lie energetically below the initial level.

In a next step each $A\,^1\Pi$ vibrational level has been excited and the time course of the closest triplet state has been measured. The rise times are prompt within our time resolution of 0.8 ns and the decays are monoexponential and span a range of 10–1000 ns (Table II). In Sec. III B it will be shown that the lifetimes of the $A\,^1\Pi$ levels are shorter than 0.1 ns due to nonradiative relaxation. Therefore the prompt rises are attributed to the population times and the decay times correspond to the lifetimes of the triplet levels. The radiative lifetimes in the gas phase for these triplet states are typically several 1000 ns (Table II). The observed rate constants for the decay of the triplet states are therefore a sum of a smaller radiative and a significantly larger nonradiative relaxation rate constant.

There has to be a sort of stepwise relaxation cascade because all the lower levels remain in the emission spectra (Figs. 1 and 2) when the excitation energies are increased from the closest $A\,^1\Pi$ level to higher $A\,^1\Pi$ levels. Therefore the time course of successive triplet levels has been analyzed. We start with the pair $d(7)$ and $e(3)$ which are successive levels in the cascade (Fig. 1). Excitation of $e(3)$ via the closest $A(2)$ level yields a prompt rise and a decay with the lifetime of about 1308 ns (Table II). The lifetime is comparable to the time interval of 960 ns between the Synchrotron radiation pulses. Therefore the population decays only partly until the next excitation pulse and the rise starts from a rather large accumulated background. Excitation of $e(3)$ via the next higher level $A(3)$ results in a very slow rise time [Fig. 4(a)]. There has to be a long-living level in between $A(3)$ and $e(3)$. The closest radiating level to $A(3)$ is $d(7)$ which shows a prompt rise and a decay with 273 ns [Fig. 4(a), Table II]. This level lies above $e(3)$ (Fig. 1) and could be the precursor.

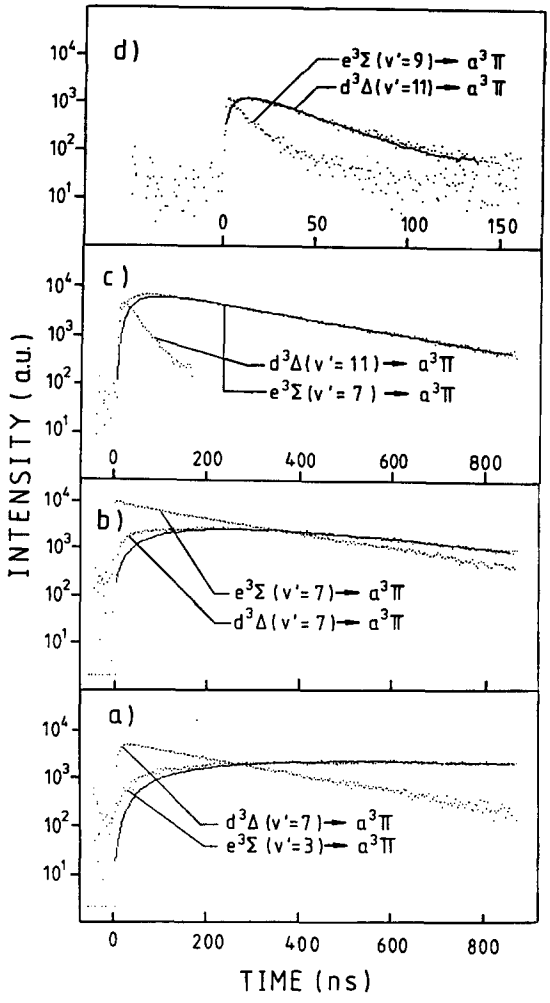

FIG. 4. Experimental time courses (points) for several transitions to $a\,^3\Pi(v''=0)$ for excitation of $v'=3$, 5, 6, and 6 of $A\,^1\Pi$ (a) to (d), respectively. A convolution of the decay times of the energetically lower levels [$e(3), d(7), e(7), d(11)$] in (a) to (d) with the time course of the higher levels [$d(7), e(7), d(11), e(9)$ in (a) to (d)] according to Eq. (2) is shown as solid line. The accumulated background in Eq. (3) has been subtracted from the experimental data for the comparison.

TABLE II. Decay rates K_{tot} of emitting triplet levels for excitation of the next higher $A\,^1\Pi$ level compared with the gas-phase radiative triplet–triplet rate constant γ_0. The decay rate of the precursor corresponds to the population rate in the cascade. All rate constants in $10^6\ s^{-1}$.

Emitting state	Decay rate in Ne	Radiative decay rate, gas	Triplet precurser in cascade
$e12$	5.42	0.303	
$e9$	111/16.9	0.303	$e12$
$d11$	51.5	0.217	$e9$
$e7$	3.66	0.303	$d11$
$d7$	3.94	0.217	$e7$
$e3$	0.76	0.303	$d7$
$d3$	1.33	0.217	
$e0$	<1	0.303	
$a'5$	<1	0.270	

The accumulated background has to be included in a quantitative analysis. The intensity $g(t)$ at time t is composed of the remaining contributions from all previous bunches

$$g(t) = g_1(t) + g_2(t) + \cdots \qquad (1)$$

with $g_1(t)$ from the last bunch, $g_2(t)$ from the second to the last, and so on. $g_1(t)$ has been derived from a convolution of

an exponential decay $e^{-t/\tau}$ with the measured time course $f_1(t)$ of the assumed precursor level:

$$g_1(t) = \int_0^t e^{-(t-t')/\tau} f_1(t')dt'. \quad (2)$$

$g_N(t)$ for the Nth earlier bunch is equal to g_1 but shifted by $N \cdot T$ with the repetition time T. Details in $f_N(t)$ are washed out for the earlier bunches at time t and f_N is approximated by e^{-t/τ_0} with the decay time τ_0 of the precursor from Table II:

$$g(t) = g_1(t) + \left[\frac{1}{K}\sum_{N=1}^{\infty} e^{-NT/\tau}\right] e^{-t/\tau} - \left[\frac{1}{K}\sum_{N=1}^{\infty} e^{-NT/\tau_0}\right] e^{-t/\tau_0}, \quad (3)$$

$$K = 1/\tau_0 - 1/\tau.$$

A fit with a variation of the $e(3)$ lifetime τ yields the original lifetime obtained for excitation of $A(2)$ and the result is plotted as solid curve in Fig. 4(a). Only the $g_1(t)$ term of Eq. (3) is shown in the experimental and calculated spectra of Fig. 4 to suppress the background. Obviously $d(7)$ is a precursor of $e(3)$ and the population time of $e(3)$ is mainly determined by the lifetime of the $d(7)$ state. This does not exclude that there are further intermediate levels in the cascade. The residence times in further intermediate levels have to be shorter than the $d(7)$ lifetime. The deviation between the fit and the experimental rise time for $e(3)$ indicates that there is an additional and faster contribution. Part of it could be due to an additional relaxation route parallel to $d(7)$. Most probably it is a spurious contribution from CO molecules in a different site. The relaxation rate constants in these sites are faster than those of the main site which will be shown in Sec. III C. The main site has been excited for the data of Fig. 4. But there is a small overlap with the wing of the second site which prohibits a complete separation. It is shown in the same way in Fig. 4(b) that $e(7)$ is a precursor to $d(7)$ for excitation of A(5). Excitation of $A(6)$ [Figs. 4(c),4(d)] initiates emission from $e(9)$ and $d(11)$. Figure 4(c) demonstrates that $d(11)$ is the precursor for $e(7)$ and Fig. 4(d) shows that $e(9)$ feeds $d(11)$. Again the lifetime of the higher level corresponds to the rise time of the next lower one. There is a complication with $e(9)$ because the decay contains two contributions, a fast one with 10 ns and a longer one with 59 ns. Both have about an equal time integrated intensity. Excitation of $A(8)$ leads to the same decay times for $e(12)$ and the lower level $e(9)$. The lifetime of $e(9)$ itself is very short compared to that of $e(12)$. In a cascade the shorter time appears as rise time, the longer one as decay time independent of the fact which one is the physical population or depopulation time. Therefore the short decay time of $e(9)$ is seen in the rising part of $e(9)$ and the long decay time of $e(12)$ appears in the decay of $e(9)$. With time resolved data the information in Fig. 1 can be completed by the decay times of each level. In addition the decay time of each higher level yields the population time of each lower level. Additional intermediate levels which perhaps do not show up in the spectra are crossed in times faster than these population times.

B. Emission bands from 130–250 nm

This region covers the spin allowed transitions from the $A\,^1\Pi$ state to the ground state and the spin forbidden transitions from the triplet states to the ground state (Fig. 1). A collection of the emission spectra for excitation of $A\,^1\Pi$ ($v' = 0,1,\ldots,8$) is shown in Fig. 5 and Table III. Each spectrum extends on the high energy side up to the stray light peak from the excitation wavelength and on the low energy side up to the $a\,^3\Pi(v'=0) \rightarrow X\,^1\Sigma_g^+$ ($v''=0$) Cameron band. The $a(0) \rightarrow X(v'')$ progression has been omitted because its intensity is about a factor 1000 higher than anyone of the bands in Fig. 5 and also since they are well known.[27] Stray light from this progression and the excitation wavelength causes the continuous background below the peaks. The widths are mainly due to the experimental resolution. The assignments, peak positions, and integrated intensities relative to the $a(0)$ Cameron bands are collected in Table III.

A general feature of all the spectra in Fig. 5 is that all progressions seen for excitation of a lower $A\,^1\Pi(v')$ state show up also for a larger v' with similar intensity. An increase of v' adds new progressions and the former ones remain. This demonstrates again that the relaxation cascade proceeds through all the lower emitting levels.

1. $A\,^1\Pi(v'=0)$

Population of $A\,^1\Pi(v'=0)$ leads to seven progressions [Fig. 5(a)] starting from $A\,^1\Pi(v'=0)$, $e\,^3\Sigma(v'=0)$, $a\,^3\Delta(v'=3)$, $a'\,^3\Sigma(v'=5)$, and from $a\,^3\Pi(v'=0,\ 1,\ 2)$ [Fig. 5(a) and Table III]. The lifetime of the $A(0)$ band is shorter than the experimental resolution of about 0.8 ns. The total intensity of 1.85×10^{-3} (Table III) in the $A(0)$ progression shows that the $A(0)$ state is depopulated predominantly nonradiatively. The radiative lifetime in the gas phase is about 8×10^{-9} s[18] and from the intensity (Table III) a lifetime of about 10^{-11} s is estimated due to nonradiative decay assuming a quantum efficiency of the Cameron band near unity. The band positions are shifted to the red by about 15–20 meV compared to the gas phase in agreement with the absorption data. The intensity distribution in the progression is well represented by the gas phase Franck–Condon factors.

The transition energies of the $e(0)$ progression are close to the gas phase values (shift between 0–5 meV). The time resolved measurements give a lower level for the lifetime of 1×10^{-6} s. It is not far from the radiative lifetime in the gas phase of 3×10^{-6} s which is due to triplet–triplet transitions. The low intensity indicates that the radiative triplet–singlet transition to the ground state is about 10^3 times weaker than the triplet–triplet radiative decay because of spin selection rules. The intensity distribution does not agree with the calculated Franck–Condon factors. The transition is induced by mixing with the $A\,^1\Pi$ state and for very small energy separation with the perturbing level a deviation from the Franck–Condon pattern is expected.[28,33] The energy separation is small in the case of the $e\,^3\Sigma$ and $d\,^3\Delta$ states and it is larger for the $a\,^3\Pi(v'=0)$ $a'^3\Sigma(v'=5)$ states which behave regularly.

On the short wavelength side of the bands of the

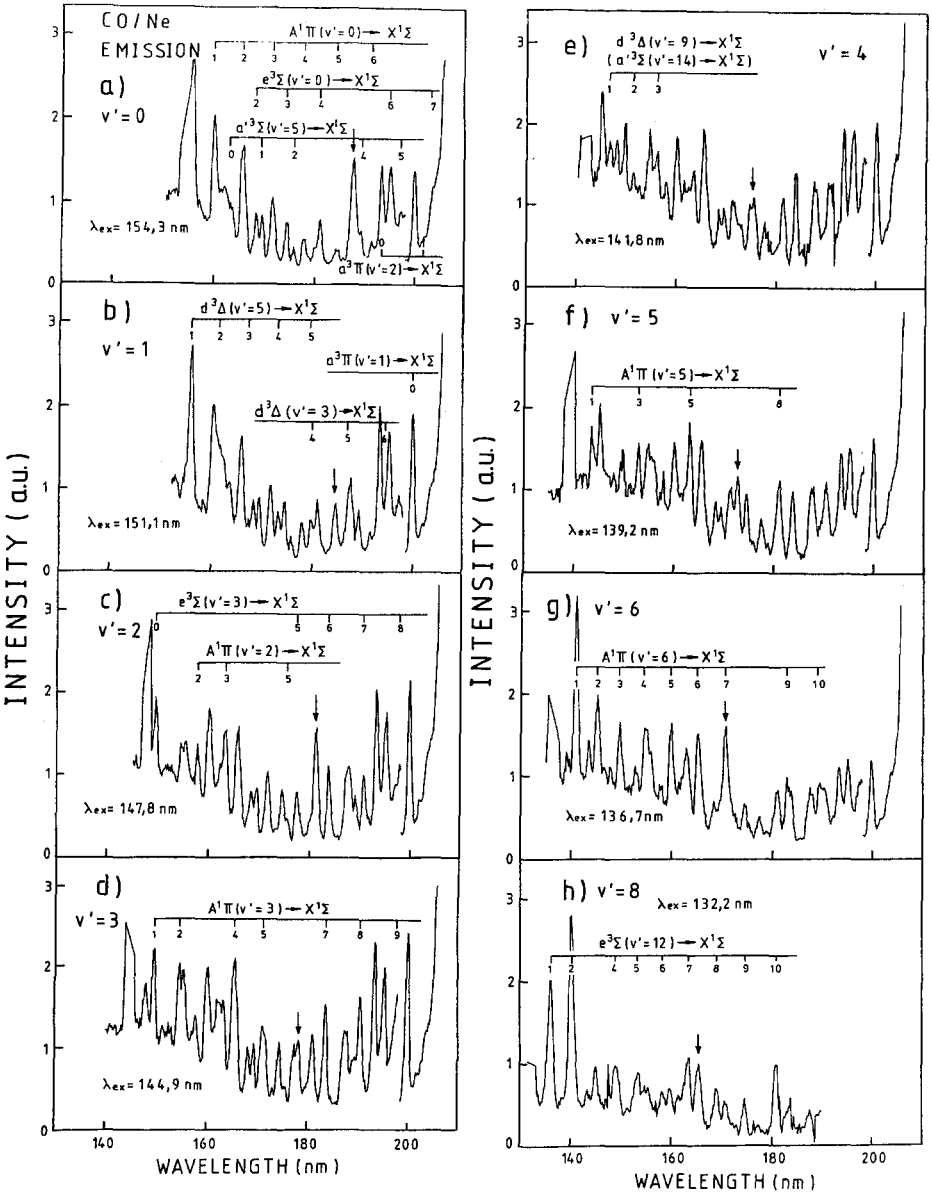

FIG. 5. VUV emission spectra for excitation of $v' = 0, 1, 2, 3, 4, 5, 6$, and 8 of $A\,^1\Pi$ for (a) to (h), respectively, corrected for the wavelength dependence of the detection system. Only the additional appearing progressions for a higher v' level are assigned. The arrows indicate a straylight peak in each spectrum.

$e\,^3\Sigma(v'=0) \rightarrow X\,^1\Sigma$ progression the transitions $d\,^3\Delta(v'=3) \rightarrow X\,^1\Sigma(v''=4, 5, 6)$ can be identified. Compared to the gas phase the transition energies are red shifted by about 7 meV. The transition energies of the $a'(5)$ progression are again close to the gas phase values (within about 5 meV) and the measured lifetimes are longer than 10^{-6} s in agreement with the triplet–triplet radiative lifetimes in the gas phase (Table II). The weak intensity indicates again that only about 10^{-3} of the intensity follow the spin forbidden radiative route to the ground state. In this case of a singlet–triplet transition the intensities and Franck–Condon factors are in accordance. The bands at 199.90 and 193.46 nm finally are the first members of progressions starting from $v' = 1$ and $v' = 2$ of $a\,^3\Pi$ and terminating at $v'' = 0$ of $X\,^1\Sigma_g$. The higher v'' members are burried under the high intensity from $v' = 0$ of $a\,^3\Pi$. From the previous information it is evident (Sec. III A) that $v' = 0, 1, 2$ are populated partly by radiative triplet–triplet transitions all with comparable intensity. The lower intensity (Table III) of the $v' = 1, 2$ levels suggests an $\sim 10^3$ times faster vibrational relaxation rate compared to the radiative decay rate to the ground state. The radiative lifetime of 0.09 s[27] gives vibrational relaxation times of about 2×10^{-4} s and 5×10^{-4} s for the $v' = 1$ and 2 level, respectively. These times are about one order of magnitude faster than radiative infrared transition times[29] and correspond therefore mainly to nonradiative vibrational relaxation times.

The states emitting in this region are indicated in Fig. 1 by wavy ($A\,^1\Pi \rightarrow X\,^1\Sigma$) and dashed (triplet–singlet) arrows in addition to the straight arrows for the visible transitions. It has to be stressed again that the starting and terminating states are unambiguously identified but in between further levels can be touched with rate constants so fast that they do not contribute significantly to the time course.

2. $A\,^1\Pi$ ($v' = 1$)

A further progression is observed which can be attributed either to $A(1)$ or to $d(5)$ according to the energies. The Franck–Condon factors do not agree with $A(1)$ and the

TABLE III. Observed VUV emission bands (in nm) for excitation of $A\,^1\Pi$ ($v' = 0, 1, 2, 3, 4, 5, 6, 8$) with the red shift in meV compared to the gas phase in brackets. The last row gives the integrated intensity of a progression relative to the integrated intensity of the $a\,^3\Pi(v' = 0) \rightarrow X\,^1\Sigma(v'')$ progression which has a quantum efficiency near unity.

Exc. to $A\,^1\Pi$	Emit. state	Emission to $X\,^1\Sigma$ (v'') 0	1	2	3	4	5	6	7	8	9	Int. (10^{-3})
$v'=0$	$A0$	154.8(19)	160.05(16)	165.66(16)	171.66(19)	177.86(15)	184.56(16)	[191.46(9)]				1.85
	$e0$		[162.26(−7)]	168.36(7)	174.46(6)	180.96(5)	[187.59(−5)]	195.16(3)				1.62
	$a'5$	163.59(7)	169.46(4)	175.86(8)		189.39(−2)	197.20(4)					2.97
	$a1$	199.90(21)										5.47
	$a2$	193.46(23)										1.92
$v'=1$	$d5$	?	156.09(−4)	[161.4(−4)]	167.39(11)	173.22(5)	179.79(14)					1.43
$v'=2$	$e3$	149.59(11)					[177.49(19)]	183.85(12)	190.89(14)	198.2(11)		1.13
	$A2$	148.00(14)		157.99(16)	163.49(21)		[175.79(43)]					1.68
$v'=3$	$A3$	(21)	(13)	(20)		(32)	(34)		(31)	(29)	(29)	2.04
	$e5$	$145.10_{(9)}$	$149.60_{(1)}$	$154.62_{(8)}$		[165.51(20)]	$171.31_{(22)}$]		$183.81_{(19)}$	$190.61_{(17)}$	$197.92_{(17)}$	
$v'=4$	$a'14$		146.80(23)	151.40(17)	156.21(10)							0.28
$v'=5$	$A5$	139.39(9)	143.46(−4)		152.86(6)		163.06(6)			181.06(24)		2.79
$v'=6$	$A6$	137.01(16)	141.20(20)	[145.20(0)]	[149.80(3)]	[154.71(10)]	160.00(22)	165.30(22)	[171.1(30)]		183.0(18)	8.68
$v'=8$	$e12$		(7)	(16)		(26)	(8)	(−2)	(6)	(9)	(−3)	
	$A8$		$136.25_{(14)}$	$140.44_{(23)}$		$149.34_{(34)}$	$153.64_{(15)}$	$158.34_{(5)}$	$163.64_{(13)}$	$169.14_{(16)}$	$174.4_{(4)}$	7.62

dominant contribution originates from $d(5)$ [Fig. 5(b)]. It seems to be a contradiction that $d(5)$ is observed in a singlet–triplet transition but not in the triplet–triplet region, discussed in Sec. III A. $d(5)$ is nearly resonant with $A(1)$ and from the gas phase a strong mixing of these states is known.[17] It adds a singlet character to $d(5)$, which enhances strongly the $d(5)$–$X\,^1\Sigma$ radiative transition rate (Sec. IV C). The induced $d(5) \rightarrow X\,^1\Sigma_g$ radiative transition rate of 3×10^{-6} s (Table IV) corresponds to a lifetime of about 5×10^{-9} s of $d(5)$ according to the weak intensity (Table III). The inten-

TABLE IV. Calculated radiative rates γ_{TS} [Eq. (9)] for transitions of triplet states to $X\,^1\Sigma$ ground state due to a perturbing $A\,^1\Pi$ level with gas phase spin–orbit coupling matrix elements V [Eq. (11)], energy differences δ, and mixing coefficients in the matrix β_M [Eq. (13)]. The model is correct provided the ratio γ_{TS}/K_{tot} (with K_{tot} from Table II) corresponds to the ratio I_{TS}/K_{tot} with the triplet intensity I_{TS} and the total intensity (Cameron bands) I_{tot} from Table III. The categories A, B, C distinguish between levels for which triplet–singlet and triplet–triplet (A), or only triplet–singlet (B), or only triplet–triplet transition (C) have been observed (all rate constants in $10^6\ s^{-1}$).

Emit. state	Pert. level	V (cm^{-1})	δ (meV)	β_M^2	γ_{TS} ($10^6 \cdot 1/s$)	k_{tot} ($10^6 \cdot 1/s$)	$\frac{\gamma_{TS}}{k_{tot}}$	$\frac{I_{TS}}{I_{tot}}$	Category
$e3$	$A1$	−2.07	87.3	$1.08E-5$	$1.03E-2$	0.764	$1.35E-2$	$1.1E-3$	A
	$A2$	+8.0	−92	$9.19E-5$					
$e12$	$A8$	4.03	−7.2	$2.00E-3$	$2.00E-1$	5.55	$3.60E-2$	$4.5E-3$	A
$d3$	$A0$	14.5	−91.2	$3.25E-4$	$3.25E-2$	1.33	$2.44E-2$	$1.53E-3$	A
	A_0	5.975	−129	$2.70E-5$					
$e0$	$A1$	11.32	−313	$1.78E-5$	$5.58E-3$	0.303	$1.84E-2$	$1.62E-3$	B
	$A2$	13.95	−492	$1.10E-5$					
	$A0$	−4.85	−442	$1.62E-6$					
$a'5$	$A1$	+7.35	−626	$1.87E-6$	$3.74E-4$	0.270	$1.38E-3$	$2.97E-3$	B
	$A2$	−3.42	−805	$2.47E-7$					
$d9$	$A4$	4.04	−24.8	$2.63E-4$	$2.63E-2$	>100	$<2.63E-4$	$0.3E-3$	B
$a'14$	$A4$	4.21	−2.6	$1.26E-2$	$1.26E0$	>100	$<1.26E-2$	$0.3E-3$	B
$e5$	$A3$	5.51	−12.4	$1.54E-3$	$1.54E-1$	>100	$<1.54E-3$	$2.0E-3$	B
$d5$	$A1$	9.77	−6.9	$1.26E-2$	$1.26E0$	>100	$<1.26E-2$	$1.4E-3$	B
$d7$	$A2$	−6.2	72.1	$1.51E-4$	$1.55E-2$	3.94	$3.93E-3$		
	$A3$	−1.41	−103	$3.64E-6$					
$e7$	$A4$	+4.41	62.0	$1.10E-4$	$1.13E-2$	3.66	$3.09E-3$		
	$A5$	+1.3	−105	$2.98E-6$					
								$<5E-4$	C
$d11$	$A5$	−1.74	48.4	$3.24E-5$	$7.79E-3$	52.5	$1.48E-4$		
	$A6$	+6.57	−114	$4.55E-5$					
$e9$	$A6$	−0.72	−31.0	$2.26E-5$	$2.83E-3$	111/16.9	$2.55E-5$		
	$A5$	−3.94	+131	$5.70E-6$			$1.67E-4$		
$e11$	$A7$	+2.36	37.4	$1.65E-4$	$1.84E-2$	...	...		
	$A8$	−4.78	−117	$1.92E-5$					

TABLE V. Calculated intersystem crossing rate constant $K^{cal}_{ST'}$ [Eqs. (15) and (16)] from an $A\,^1\Pi$ level to the next triplet level with the electronic $A(cm^{-1})$ and vibrational $\langle v'|v\rangle$ part ot the intramolecular matrix element, the energy gap δ (meV) and the phonon Franck–Condon factor $\langle p'|0\rangle$ [Eq. (14)] compared to the experimental rate constants $K^{exp}_{ST'}$ from the $A\,^1\Pi$ emission intensity. All rate constants in $10^9\ s^{-1}$.

Transition	$A(cm^{-1})$	$\langle v'\|v\rangle^2$	δ(meV)	$\langle p'\|0\rangle^2$	$K^{cal}_{ST'}(10^9\cdot 1/s)$	$K^{exp}_{ST'}(10^9\cdot 1/s)$
$A\,0/a'8$	21	$0.587E-2$	37.5	$0.139E-2$	$0.903E-1$	$0.540E2$
$A\,0/I0$	0.2	$0.447E-1$	25.1	$0.278E-1$	$0.124E-2$	$0.540E2$
$A\,1/d\,5$	34	$0.966E-1$	6.9	$0.328E0$	$0.915E3$	$>0.200E3$
$A\,2/a'11$	21	$0.247E-1$	18.1	$0.103E0$	$0.280E2$	$0.595E2$
$A\,3/e5$	25	$0.651E-1$	12.4	$0.230E0$	$0.234E3$	$0.490E2$
$A\,4/a'14$	21	$0.365E-1$	2.6	$0.304E0$	$0.122E3$	$>0.200E3$
$A\,5.a'15$	21	$0.436E-1$	53.2	$0.113E-4$	$0.545E-2$	$0.358E2$
$A\,5/I\,7$	0.2	$0.201E-1$	24.5	$0.332E-1$	$0.668E-3$	$0.358E2$
$A\,6/d\,12$	34	$0.176E-1$	-2.5	$0.273E0$	$0.139E3$	$0.115E2$
$A\,7/a'18$	21	$0.389E-1$	39.7	$0.593E-3$	$0.254E0$	$>0.200E3$
$A\,7/d\,13$	34	$0.309E-1$	41.5	$0.425E-3$	$0.379E0$	$>0.200E3$
$A\,7/I\,10$	0.2	$0.343E-1$	6.9	$0.328E0$	$0.113E-1$	$>0.200E3$
$A\,8/e12$	25	$0.815E-2$	7.2	$0.318E0$	$0.405E2$	?

sity in the $d(5)\rightarrow a\,^3\Pi$ triplet–triplet transition with its typical radiative lifetime of 5×10^{-6} s would be too low to be detected.

3. $A\,^1\Pi\,(v'=2)$

Two additional progressions starting from $A(2)$ and $e(3)$ are observed [Fig. 5(c)]. $e(3)$ showed up also in the visible [$e(3)\rightarrow a\,^3\Pi$] and the time courses are identical in both cases. The $e(3)$ lifetime of 1.3×10^{-6} s is long, therefore the spin forbidden $e(3)\rightarrow X\,^1\Sigma_g$ transition is detectable despite only weak mixing (Table IV).

4. $A\,^1\Pi\,(v'=3)$

Only the weak $A(3)$ emission bands with intensities similar to the Franck–Condon factors are new in the spectrum of Fig. 5(d).

5. $A\,^1\Pi\,(v'=4)$

The new progression is assigned alternatively to $d(9)$ superimposed on $a'(14)$. $A(4)$ is excluded because of Franck–Condon factors and $d(7)$ which has been seen in the visible should have appeared earlier for excitation of $A(3)$. $a'(14)$ is nearly resonant with $A(4)$. Its appearance in the UV and the absence in the triplet–triplet region is again attributed to strong mixing with $A(4)$ (Table IV).

6. $A\,^1\Pi\,(v'=5,\ v'=6,\ v'=7)$

Only $A(5)$and $A(6)$ progressions are identified [Figs. 5(f) and 5(g)]. The assignment is supported by the Franck–Condon factors and the subnanosecond lifetime. No further bands show up for $v'=7$.

7. $A\,^1\Pi\,(v'=8)$

A progression due to $A(8)$ is observed [Fig. 5(h)]. The bands at 136.25 and 140.4 nm belong to a progression starting from $e(12)$ and show the same time coures as the corresponding triplet–triplet transitions from $e(12)$ in the visible. Some further members are covered partly by the $A(8)$ progression.

The UV spectra yielded important information on the A states in the cascade as can be seen from Fig. 1. Several of them have been observed. All of them are depopulated nonradiatively very fast by intersystem crossing. $A(0, 2, 3, 5, 6, 8)$ with a rate constant of about 10^{11} to $10^{10}\ s^{-1}$ and $A(1, 4, 7)$ even faster (Table V) according to the intensities in Table III. Vibrational relaxation within the $A\,^1\Pi$ manifold cannot be the dominant process for the fast depopulation because triplet states above the next lower $A\,^1\Pi$ vibrational state are populated with about 100% efficiency and a corresponding fast rise time. The lower $A\,^1\Pi$ levels are also populated with very high efficiency by reverse intersystem corssing, because they appear with unchanged intensity for excitation of any of the higher $A\,^1\Pi$ levels (Fig. 1). Some more intermediate triplet states have been identified ($a'5$,$a'14$,$e0$,$d\,5$) with radiative rate constants shortened by mixing with A states. Finally radiationless vibrational relaxation in the $a\,^3\Pi$ state with rate constants of the order of $2\text{–}5\times10^3\ s^{-1}$ has been found.

C. Excitation spectra

The intensities of some representative triplet–triplet transitions starting from $d(3)$, $d(7)$, and $e(7)$ versus the intially excited $A\,^1\Pi$ state are compared with those for the $a(0)\rightarrow X(0)$transition in Fig. 6. The spectrum for the Cameron band is in agreement with the $X(0)\rightarrow A(v')$ Franck–Condon pattern. This observation and the high intensities indicate that nearly all of the population relaxes to the $a(0)$ level. The bypass by radiative singlet–singlet and triplet–singlet transitions from higher states is only of the order of 10^{-2} (Sec. III B). The $e(3)$, $d(7)$, and $e(7)$ bands show up for the first time for excitation of the next higher $A\,^1\Pi$ level in agreement with the emission spectra of Sec. III B. In Sec. III B it has been demonstrated that higher triplet states are the precursors of lower triplet states for excitation of higher $A(v')$ levels. An efficient bypass would result in a drop in intensity in one of the excitation spectra of Fig. 6 relative to the $a(0)$ spectrum. Only about 10% are missing in the $e(3)$, $d(7)$, and $e(7)$ spectra for high $A(v')$ levels. This amount is just the expected bypass by the radiative triplet–triplet tran-

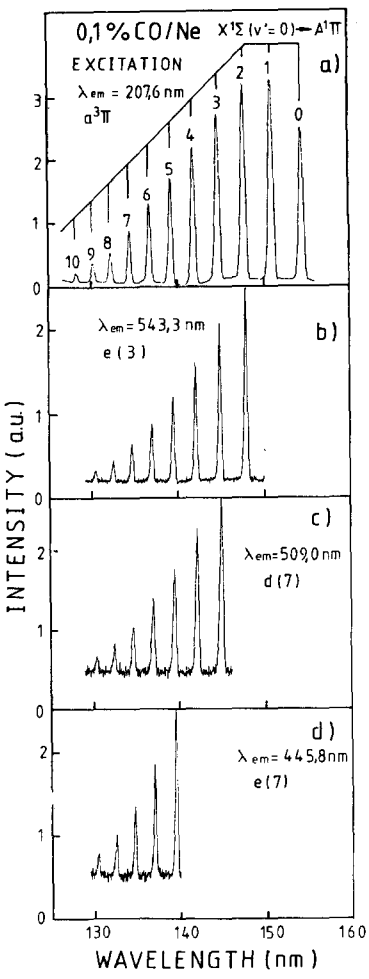

FIG. 6. Intensities in the emission bands from $a\,^3\Pi(v'=0)$ to $X\,^1\Sigma$ $(v''=0)$ [Fig. 6(a)] and from $e\,^3\Sigma(v'=3)$, $d\,^3\Delta(v'=7)$, $e\,^3\Sigma(v'=7)$ to $a\,^3\Pi(v'=0)$ [Fig. 6(b) to 6(d)], respectively), vs the excitation wavelength in the region of the $X\,^1\Sigma(v'=0)\rightarrow A\,^1\Pi(v'=0$ to 10) transitions, not corrected for the smooth wavelength dependence of the photon flux.

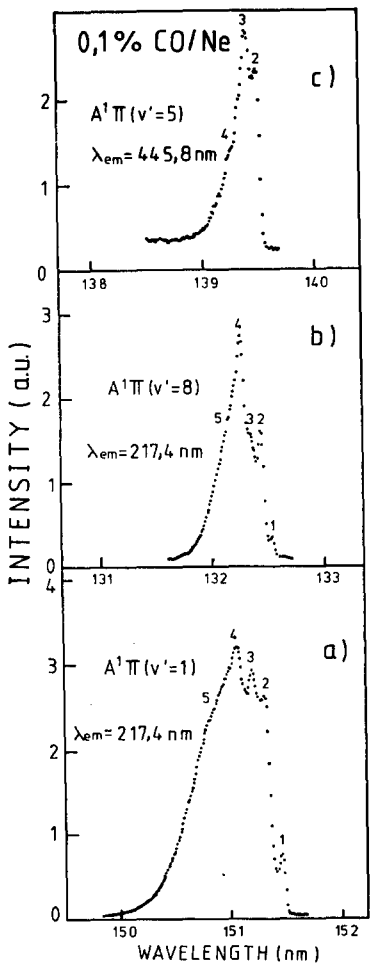

FIG. 7. Excitation spectra like in Fig. 6 but with high resolution in the region of $v'=1$, 8, and 5 absorption bands of $A\,^1\Pi$ for 6(a) to 6(c), respectively. The intensity in $a\,^3\Pi(v'=0)\rightarrow X\,^1\Sigma(v''=0)$ is recorded in Figs. 6(a) and 6(b) and that of $e\,^3\Sigma(v'=7)$ to $a\,^3\Pi(v'=0)$ in Fig. 6(c) (see the text).

sitions which have radiative rate constants of $<10^6\ s^{-1}$ whereas the typical nonradiative rate constants are much larger (Table II). The excitation spectra confirm once more that about 90% of the intensity flows nonradiatively through the emitting levels shown in Fig. 1 down to the triplet levels $a'(5)$, $e(0)$, and $d(3)$. The contribution of radiative transitions to the further *relaxation* down to $a(0, 1, 2)$ is not known because the transitions would be in the infrared.

The line shapes of a typical lower $[A(1)]$ and a higher $[A(8)]$ singlet level in excitation spectra of the Cameron bands are compared in Figs. 7(a) and 7(b) at high resolution. Four maxima (1–4) and a broad shoulder (5) are identified. The width of the shoulder 5 decreases in going from $A(1)$ to $A(8)$ and maximum 4 shifts to lower energies relative to the reference maximum 2. Also the relative intensities of 3 and 2 decrease. The excitation spectrum for a typical triplet–triplet transition $[e(7)\rightarrow a(0)]$ is qualitatively different (Fig. 7). Maximum 1 is missing and the dominant structures 4 and 5 in Figs. 7(a) and 7(b) have merged to the small shoulder 4. The spectrum 7(c) is representative for all vibrational levels of $A(v')$ and for all emitting triplet states d and e. An explanation for the observed difference in the excitation spectra is the presence of different sites of CO. One type of site which we will call the main site is responsible for the maxima 2 and 3. Another or several other sites are called minority sites cause the structures 1, 4, and 5. The main site has the properties discussed in Secs. III A and III B because the spectra have been taken for excitation just in the center between maxima 2 and 3. The minority sites have a different surrounding which leads to a faster radiationless relaxation on the A, e, and d states. The shorter radiationless lifetime for a fixed radiative lifetime reduces the amount of triplet–triplet emission from these states and they contribute less effectively to the excitation spectrum of Fig. 7(c). By radiationless processes both types relax to the $a(0)$ state. Obviously the $a(0)$ state has a high radiative quantum efficiency for main and minority sites and both types are seen in the excitation spectra Figs. 7(a) and 7(b) of the Cameron bands.

This point of view is supported by the time resolved spectra. Some time courses for the main site from Fig. 4 are compared in Fig. 8 with those for excitation near structures 4 and 5 (Fig. 7). Without going into details it is evident that indeed all rise and decay times for the minority sites are faster and they are due to radiationless processes. Unfortunately the structures for 4 and 5 are broad and overlap partly

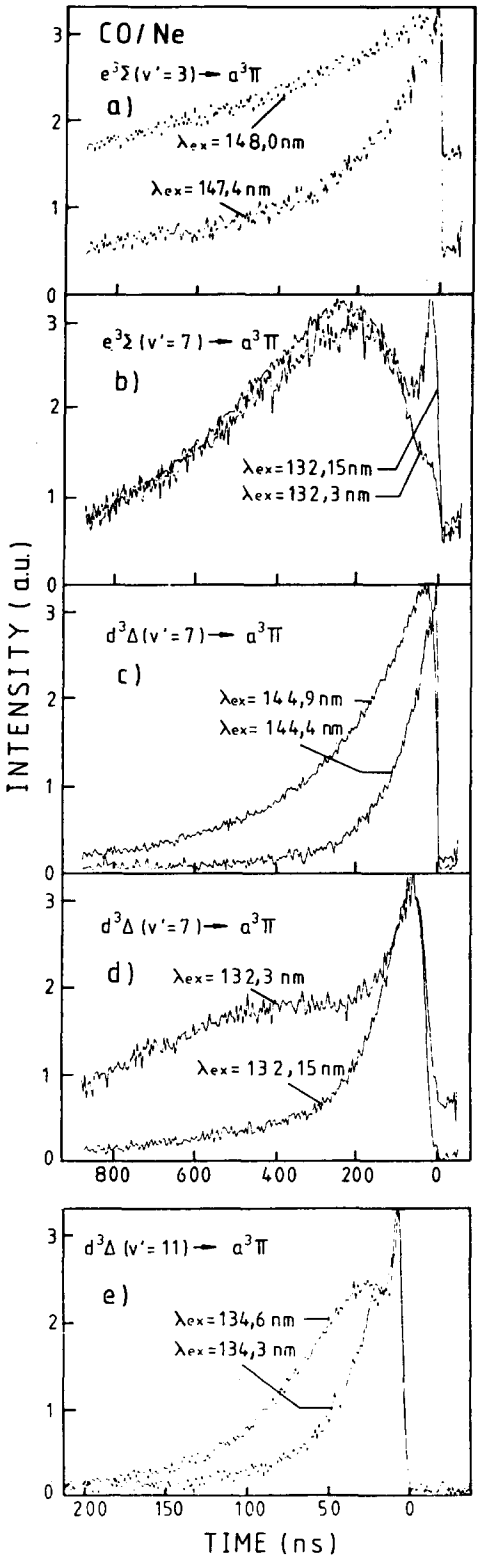

FIG. 8. Time courses of the transitions from $e\,^3\Sigma(v'=3)$, $e\,^3\Sigma(v'=7)$, $d\,^3\Delta\,(v'=7)$ $d\,^3\Delta(v'=7)$, $d\,^3\Delta(v'=11)$ to $a\,^3\Pi(v''=1)$ for (a) to (e), respectively. Excitation into the main site (larger λ_{ex}) and minority site (smaller λ_{ex}) of the $v'=2, 8, 3, 8, 7$ absorption bands of $A\,^1\Pi$ for (a) to (e), respectively.

with maximum 3. Therefore the discrimination is not complete and the fast parts in the main site spectra 8(d) and 8(e) are most probably remainders from the minority site.

In the following we will address only the main site. The separation between the two lines 2 and 3 in the excitation spectrum Fig. 7(c) is about 6–7 meV. It is close to the maximum of the phonon density in Ne. Therefore maximum 2 is attributed to the zero phonon line and maximum 3 to a phonon sideband. From the intensity a phonon coupling strength S of about 1.3 is estimated.[19] The shoulder 4 is partly a remainder from the minority site and covers perhaps higher phonon sidebands of the main site. Its contribution to 3 renders the S value uncertain between 1 and 2.

VI. DISCUSSION

A. Mixing of electronic states

First we will focus our attention on the intersystem crossing from the initial $A\,^1\Pi$ vibrational levels to the triplet manifold with rate constants larger than $10^{10}\,s^{-1}$. Such high rate constants cannot be induced by the heavy atom effect due to intermolecular CO-matrix spin–orbit coupling in the case of the light Ne collison partner. A mixing of singlet and triplet states by CO intramolecular spin–orbit coupling in combination with a collision induced relaxation can be sufficiently effective according to gas phase experiments.[14,18]

The excited singlet states S and triplet states T are of mixed electronic parentage. The mixing for the simplest case of only pairwise interacting states is given by

$$|S\rangle = \cos\theta\,|s\rangle + \sin\theta\,|t\rangle, \tag{4}$$

$$|T\rangle = -\sin\theta\,|s\rangle + \cos\theta\,|t\rangle, \tag{5}$$

with

$$\tan 2\theta = V/\delta. \tag{6}$$

$|s\rangle$ and $|t\rangle$ are pure singlet and triplet states which obey strict spin selection rules. V is the intramolecular spin–orbit coupling matrix element and $\delta = (E_s - E_t)/2$ is one-half the energy separation between the pure unperturbed states.[15,30] The triplet content $\sin\theta$ in the singlet states will be called $\beta = \sin\theta$ in the following. The mixing increases the splitting of the perturbed S and T states and the energy shifts ΔE relative to the unperturbed energies are given by

$$\Delta E = \delta \pm \sqrt{\delta^2 + |V|^2}. \tag{7}$$

The spin selection rules for radiative transitions in the mixed states are weakened. The radiative rate constants γ_s for the allowed singlet–singlet transition of the pure s states are reduced for transitions from the mixed singlet state S to the pure singlet ground state to

$$\gamma_S = (1-\beta^2)\gamma_s. \tag{8}$$

Transitions of the pure t states to the ground states are strictly forbidden with $\gamma_t = 0$. They become partly allowed for the mixed T states with

$$\gamma_{TS} = \beta^2\gamma_s. \tag{9}$$

Finally an intersystem crossing by collisons takes place between the mixed S and T states which would have been strictly forbidden for the pure states. The rate constant K_{ST} for this combined intersystem crossing and relaxation process is given within the first order perturbation theory[14,18,30] by

$$K_{ST'} = \beta^2 K_{TT'} \tag{10}$$

with a triplet relaxation rate constant $K_{TT'}$. The relaxation processes responsible for $K_{TT'}$ can be any change of the rotational, vibrational, or electronic quantum number. ΔE,[17] γ_S, and $K_{ST'}$[18,30] have been studied in detail for the $A\ ^1\Pi$ state in the gas phase. In principle these effects should also appear in the Ne matrix but with different values for β^2 and another type of triplet relaxation $K_{TT'}$. In the gas phase large β^2 values show up due to accidental energy resonances δ for certain rotational quantum numbers J in the singlet and triplet states with $\Delta J = O$. The spin–orbit coupling matrix element contains an electronic part A and the Franck–Condon factor for the involved vibrational levels v and v'[17]:

$$V = A\,\langle v'|v\rangle. \tag{11}$$

$K_{TT'}$ is attributed to a fast collision induced rotational relaxation. In the matrix $J = 0$ singlet states are prepared (Fig. 7) and for the mixing also only $J = 0$ triplet states should be relevant according to the $\Delta J = 0$ condition. The molecule in the matrix is considered to be dressed by the neighboring matrix atoms. The vibrations relative to the cage, i.e., the phonons come into play for the energy resonance conditions because there are no selection rules for vibrations. The gas phase energy difference δ between v and v' will be reduced for an initially prepared singlet zero phonon level v to $\delta_{p'} = \delta \mp p'\hbar\omega_p$ for p' phonons with energy $\hbar\omega_p$ in the triplet level v'. $-$ or $+$ stands for a triplet level below or above the singlet level.

There is a distribution of phonon energies (Fig. 7) and to avoid an artificial divergence in Eq. (13) by an accidental $\delta_{p'} = 0$ we kept all $\delta_{p'}$ larger than 1 meV. The coupling matrix element V will be extended to $V_{p'}$ according to the phonon Franck–Condon factor $\langle p'|0\rangle$:

$$V_{p'} = A\,\langle v'|v\rangle\,\langle p'|0\rangle. \tag{12}$$

Summation over a phonon progression p' yields a mixing coefficient β_M^2 in the matrix which is given for small mixing by

$$\beta_M^2 = \sum_{p'} V_{p'}^2/\delta_{p'}^2. \tag{13}$$

For the evaluation of the energy differences $\delta_{p'}$ in Eq. (13) matrix induced shifts of the levels have to be considered. The absorption and emission spectra indicate that the zero phonon lines of the $A\ ^1\Pi$, $e\ ^3\Sigma$, $d\ ^3\Delta$, and $a\ ^3\Pi$ states in transitions to the ground state are shifted to the red compared to the gas phase by 14, 12, 12, and 13 meV, respectively, with an uncertainty of 2 meV. Therefore we assume that the relative positions of the excited states are the same as in the gas phase within the experimental accuracy with a possible small red shift of $A\ ^1\Pi$. The $A\ ^1\Pi$ phonon sideband suggests a relevant phonon energy between 6 and 7 meV (Fig. 7) and we take the maximum of the phonon density of Ne for $\hbar\omega_p = 6.2$ meV.

Concerning $v_{p'}$, in Eq. (13) we assume that A and $\langle v'|v\rangle$ in the matrix are close to the gas phase values[17] since the influence of the matrix on the transition energies has also been very small. The phonon Franck–Condon factors are estimated from the electron phonon coupling strength S in the usual harmonic approximation[15,19]:

$$\langle p'|0\rangle = \exp(-S/2)(\sqrt{S})^{p'}(p'!)^{-1/2} \tag{14}$$

The transition energies and line shapes in the absorption and emission spectra are consistent with S values of 1.3 ± 0.4 for the combination of $A\ ^1\Pi$ with d, e, a' triplet states, for $a\ ^3\Pi$ with the d, e, a' states, and with S values of 0.3 for combinations between d, e, a' states. The value of 0.3 corresponds to an upper limit.

B. Energy shifts by mixing

Figure 9 gives an overview on those levels which are closest to the $A\ ^1\Pi$ vibrational levels. Strong interaction occurs between $A(1)$–$d(5)$, $A(4)$–$a'(14)$, $A(6)$–$d(12)$, and $A(8)$–$e(12)$ according to the resonance condition. The largest shift would be expected for $A(6)$ with a ΔE value of <0.1 meV from Eq. (7) according to $V \approx 0.8$ meV,[17] $V_{p'} \approx 0.3$, and $\delta \approx 2.5$ meV. The energy shifts are derived experimentally from irregularities in the sequence of vibrational spacings. The accuracy of our data is only about 1 meV and the high resolution data in Ref. 20 are also given in 1 meV digits. The data of Ref. 21 with energy positions of 0.1 meV accuracy show a shift to those of Ref. 20 by about 5 meV and a scatter of this shift by more than 1 meV for different vibrational levels. A discussion of the energy shifts has to wait until those discrepancies are solved.

C. Triplet-singlet radiative transitions by mixing

A decrease in the $A\ ^1\Pi$ radiative rate constant of $\gamma_s = 10^8\ s^{-1}$ by mixing has been studied in the gas phase.[18] The smallest possible value by a triplet content of $\beta^2 = 0.5$ would be limited to $\gamma_S = 2\times10^8\ s^{-1}$ [Eq. (8)] and this effect would be completely buried in the matrix by the much larger intersystem crossing rate constant. But the appearance of triplet–singlet radiative transitions demonstrates that we observe in the matrix a singlet content by mixing [Eq. (9)]. For each emitting triplet state from Fig. 1 and Tables I and II we listed the perturbing singlet state, the matrix element V, the energy separation δ, the mixing β_M^2 in the matrix [Eq. (13)], and the resulting radiative triplet-singlet rate constant γ_{TS} [Eq. (9)] in the matrix in Table IV. Our model is correct when the ratio γ_{TS}/K_{tot} (second last row in Table IV) of the radiative rate constant to the total rate constant K_{tot} (which includes radiationless relaxation) is equal to the ratio I_{TS}/I_{tot} (last row of Table IV) of the triplet–singlet intensity I_{TS} to the total intensity (Cameron bands) from

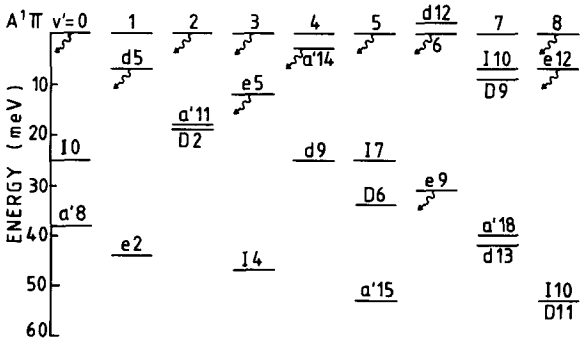

FIG. 9. Energy level scheme of the singlet ($I\ ^1\Sigma$,$D\ ^1\Delta$) and triplet levels ($d\ ^3\Delta$, $e\ ^3\Sigma$, $a'\ ^3\Sigma$) which are closest to each vibrational level v' of $A\ ^1\Pi$.

Table III. The states in Table IV are grouped in three categories A, B, C for a comparison. In category A containing e (3 and 12), we observed triplet–triplet transitions yielding K_{tot} (Table II) and we observed triplet–singlet transitions yielding I_{TS}/I_{tot}. The agreement of $\gamma_{TS}/K_{\text{tot}}$ with I_{TS}/I_{tot} is very satisfying in view of an uncertainty in β perhaps by a factor of 3 and thus a factor of 10 in β^2.

In category B triplet–singlet transitions have been seen giving I_{TS}/I_{tot} but no triplet–triplet transitions. For $e(0)$ and $a'(5)$ we know that K_{tot} is larger than 3×10^5 s^{-1} and close to the triplet–triplet radiative rate constants which are used in the $\gamma_{TS}/K_{\text{tot}}$ values of Table IV. For the other levels in B we have only a lower limit for $K_{\text{tot}} > 10^8$ s^{-1} given by the radiative triplet–triplet rate constants of about 2×10^5 s^{-1} and the limit of detection of 2×10^{-3}. The two last rows at Table IV show that the calculated γ_{TS} values are consistent with the experiment also for category B.

Finally in category C we observed triplet–triplet transitions and thus $\gamma_{TS}/K_{\text{tot}}$ but not triplet–singlet transitions. The sensitivity in the visible is higher and we can pose an upper limit of 5×10^4 for I_{TS}/I_{tot}. Again model and experiment are consistent because the inequality is fulfilled in the last two rows of Table IV within the expected accuracy. In summary, the mixing explains satisfactorily why in some cases transitions to triplet levels and to the ground state appear and why in the other cases only the one or the other transitions are strong enough.

D. Intersystem crossing

A crucial test for the model will be if Eq. (10) describes the intersystem crossing rate K_{ST} for different $A\,^1\Pi$ vibrational levels. The mixing by β_M causes a coherent superposition of singlet and triplet states and the triplet content T is scattered by $K_{TT'}$ to a real stationary triplet state T'. $K_{TT'}$ in the matrix is dominated by the fastest possible dissipation process in a phonon level p', presumably a simple one phonon relaxation to $p'-1$. This assumed one phonon process is responsible for the scattering rate constant $K_{TT'}$ and in addition the one phonon energy has to be the energy difference between the initial singlet state S and the final triplet state T' to maintain energy conservation. The summation in Eq. (13) has to be replaced by the phonon level p' which lies within one phonon energy above or below the singlet state S. The strongest perturbing triplet states for each $A\,^1\Pi$ vibrational level (Fig. 9) are listed in Table V together with the intramolecular spin–orbit coupling matrix element A, the molecular Franck–Condon factor $\langle v'|v\rangle$, and the energy difference δ. The gap δ is filled up to $\delta_{p'}$ by p' phonons with a Franck–Condon factor $\langle p'|0\rangle$ [Eq. (14)] (Table V) to derive $V_{p'}$ [Eq. (12)] and $\beta_M = V_{p'}/\delta_{p'}$. Since there is a distribution of phonon energies a mean value of 20 cm^{-1} (2.4 meV) for $\delta_{p'}$ is reasonable to avoid artificial fluctuations in β_M.

Estimates for the phonon relaxation in the solid phase are of the order of $K_{TT'} = 10^{13}$ s^{-1}. Recent experiments[31] for the dissipation of optical phonons in alkali halide color centers yielded lower limits of 1.5×10^{14} s^{-1}. We are dealing with acoustic phonons of a typical frequency of 1.4×10^{12} s^{-1}. The essential process perhaps is a dissipation of phonons away from the vicinity of the molecule into the matrix with a typical sound velocity of 7×10^{12} Å/s. If we choose $K_{TT'} = 10^{13}$ s^{-1} and $V_{p'} = 20$ cm^{-1}, we can rewrite Eq. (10):

$$K_{ST'} = |V_{p'}|^2 K_{TT'}/\delta_{p'}^2 = |V_{p'}|^2 1.6\times10^{18}\ [\text{s}^{-1}]. \quad (15)$$

The numerical values are close to the well-known result from Fermi's–Golden rule[32] $\approx$

$$K_{ST'} = 2\pi\,|V_{p'}|^2/(\hbar^2\omega_p) = |V_{p'}|^2\ 1.6\times10^{18}\ [\text{s}^{-1}]. \quad (16)$$

The scattering $K_{TT'}$ is sufficiently strong that we are in the statistical limit[14] and a further increase in $K_{TT'}$ would not accelerate anymore the relaxation. The intersystem rate constants $K_{ST'}^{\text{cal}}$ in the second last row of Table V are calculated from $V_{p'}$ according to Eqs. (15) or (16).

Emission from $A(0)$, $A(2)$, $A(3)$, $A(5)$, $A(6)$, and $A(8)$ has been observed and from the intensity (Table III) together with the radiative lifetime we get the experimental rate constants $K_{ST'}^{\text{exp}}$ in the last row of Table V. The agreement within one order of magnitude is encouraging. Emission from $A(1)$ and $A(4)$ was too weak to be detected and from the limit of detection a lower limit for $K_{ST'}^{\text{exp}} > 2\times10^{11}$ s^{-1} is induced in Table V. The inequality is convincingly fullfilled by the calculated rates.

But for $A(0)$, $A(5)$, and $A(7)$ the calculated intersystem crossing rate constants are two to three orders of magnitude too small compared to the experiment. Inspection of Fig. 9 shows that these are the only cases where a singlet level [$I(0)$, $I(7)$, and $I(10)$] lies within the gap between the $A\,^1\Pi$ level and the perturbing triplet level. The first step will be an internal conversion to the corresponding $I\,^1\Sigma^-$ level and the next step an intersystem crossing. An estimate of the internal conversion rate constants $K_{SS'}^{\text{cal}}$ with the intramolecular matrixelement (Table V, Ref. 17) in the same framework yields values which are again about four orders of magnitude too low. But internal conversion can be induced by any nonadiabatic matrix element A_{na} for example due to the interaction with the matrix. If A_{na} would be of the same order of magnitude as the spin–orbit coupling matrix elements ($\sim$20 cm^{-1}) instead of the small intramolecular matrix elements of 0.2 cm^{-1} (Table V) β would increase by 10^2, β^2 by 10^4, and accordingly $K_{SS'}^{\text{cal}}$ by 10^4 in agreement with the experiment (Table V).

The model provides an order of magnitude description of the intersystem crossing rate constants. Therefore an application to internal conversion in the triplet states like above for the singlet states has to be tested. In this context it is worth noting that the gas phase theoretical and experimental cross sections for CO/He and CO/Ne of about 1 Å^2 for $\beta^2 = 0.005$[18,30] also lead to intersystem crossing rate constants of about 10^{10} s^{-1} for an extrapolation to the solid matrix density.

E. Internal conversion, intersystem crossing, and bottlenecks in triplet states

In a first step it will be checked if the model is able to predict the experimentally observed bottlenecks in the d and

TABLE VI. Calculated internal conversion rate constants K_T^{cal} for $e\,^3\Sigma$ and $d\,^3\Delta$ states with A, $\langle v'|v\rangle$, δ, and $\langle p'|0\rangle$ like in Table V compared to K_{tot} (Table II) or the lower limit of $10^8\ s^{-1}$. All levels with $K_{TT'}^{cal} < 10^8\ s^{-1}$ or those which have been observed in emission are identified as bottlenecks (all rate constants in $10^9\ s^{-1}$).

Transition	A (cm^{-1})	$\langle v'/v\rangle^2$	δ (meV)	$\langle p'/0\rangle^2$	Calc. rate ($10^9\cdot 1/s$) Fast relaxation	Calc. rate ($10^9\cdot 1/s$) Bottle-neck	Expt. rate ($10^9\cdot 1/s$) Bottle-neck	Expt. rate ($10^9\cdot 1/s$) Fast relaxation
$d\,1/a8$	25	$0.742E-1$	49.5	$0.557E-4$	$0.646E-1$			$>0.1E0$
$d\,2/a9$	25	$0.138E0$	6.0	$0.351E0$	$0.758E3$			$>0.1E0$
$d\,3/e0$	20	$0.501E-7$	38.2	$0.314E-6$		$0.157E-9$	$0.133E-2$	
$d\,4/A\,0$	34	$0.133E0$	44.0	$0.207E-3$	$0.797E0$			$>0.1E0$
$d\,5/a11$	25	$0.637E-2$	55.0	$0.870E-5$		$0.866E-3$	$>0.1E0$	
$d\,6/a12$	25	$0.590E-2$	12.5	$0.224E0$	$0.207E2$			$>0.1E0$
$d\,7/A\,2$	34	$0.521E-1$	72.1	$0.182E-7$		$0.274E-4$	$0.394E-2$	
$d\,8/A\,3$	34	$0.669E-2$	22.7	$0.398E-1$	$0.769E1$			$>0.1E0$
$d\,9/a14$	25	$0.853E-2$	54.6	$0.914E-5$		$0.122E-2$		$>0.1E0$
$d\,10/a15$	25	$0.899E-3$	13.5	$0.178E0$	$0.250E1$			$>0.1E0$
$d\,11/A\,5$	34	$0.279E-2$	48.4	$0.631E-4$		$0.509E-2$	$0.526E-1$	
$d\,12/A\,6$	34	$0.176E-1$	2.5	$0.303E0$	$0.154E3$			$>0.1E0$
$d\,13/a17$	25	$0.360E-2$	49.6	$0.551E-4$		$0.310E-2$		$>0.1E0$
$d\,14/a18$	25	$0.159E-2$	10.2	$0.255E0$	$0.634E1$			$>0.1E0$
$a'5/a7$	18	$0.364E-1$	164.3	$0.505E-25$		$0.149E-22$	$0.27E-3$	
$a'14/a14$	21	$0.365E-1$	-2.6	$0.273E0$		$0.823E-6$		
$e0/a9$	18	$0.380E-2$	105.4	$0.663E-13$		$0.204E-11$	$0.153E-3$	
$e1/A\,0$	25	$0.135E0$	6.6	$0.340E0$	$0.716E3$			$>0.1E0$
$e2/a11$	18	$0.512E-1$	18.3	$0.102E0$	$0.422E2$			$>0.1E0$
$e3/I\,2$	20	$0.186E-1$	33.1	$0.370E-5$		$0.689E-3$	$0.764E-3$	
$e4/A\,2$	25	$0.810E-1$	36.5	$0.196E-2$	$0.248E1$			$>0.1E0$
$e5/a13$	18	$0.124E0$	61.8	$0.106E-5$		$0.106E-2$	$>0.1E0$	
$e6/a14$	18	$0.644E-1$	19.9	$0.647E-1$	$0.338E2$			$>0.1E0$
$e7/I\,6$	20	$0.488E-1$	37.5	$0.548E-6$		$0.268E-3$	$0.366E-2$	
$e7/A\,4$	25	$0.481E-1$	61.9	$0.105E-5$		$0.786E-3$	$0.366E-2$	
$e8/A\,5$	25	$0.100E-1$	14.5	$0.150E0$	$0.234E2$			$>0.1E0$
$e9/a16$	18	$0.820E-1$	56.7	$0.359E-5$		$0.238E-2$	$0.111E0$	
$e10/a17$	18	$0.667E-1$	16.3	$0.120E0$	$0.650E2$			$>0.1E0$
$e11/A\,7$	25	$0.141E-5$	37.4	$0.154E-2$		$0.34E-4$	$>0.1E0$	
$e12/I\,11$	20	$0.966E-1$	46.3	$0.428E-8$		$0.414E-5$	$0.543E-2$	

e vibrational levels (Fig. 1). They are defined by the fact that the total rate constant K_{tot} (Table VI) is sufficiently small that the radiative decay is able to compete within our limit of detection. In the other cases we can give only a lower limit $K_{tot} > 10^8\ s^{-1}$ (Table VI).

The triplet states are mixed with one another and with the singlet states by spin–orbit interaction with a matrix element of about $20\ cm^{-1}$ [17] (Table VI). The internal conversion rate constants K_T^{cal} are calculated according to the same procedure [Eqs. (15) and (16)] as for K_{TS} with A, $\langle v'|v\rangle$, δ, p', and $\langle p',0\rangle$ from Table VI. Those levels with $K_{TT'}^{cal}$ or K_{TS}^{cal} smaller than $10^8\ s^{-1}$ are identified as bottlenecks. The comparison in Table VI shows that indeed all observed bottlenecks are predicted by the model which is quite satisfying. In the opposite direction also almost all calculated bottlenecks have been seen in the experiment with only two exceptions $d(9)$ and $d(13)$. This is not too disturbing because it is difficult to exclude in the experiment that some bands have been overseen due to other progressions in the same spectral range and the calculated rate constants are close to the limit of detection. Furthermore the triplet levels are populated only indirectly via the relaxation cascade from the $A\,^1\Pi$ levels and their strength in the experiment will be weighted with the branching ratio in the population flow (Sec. IV F).

The calculation identifies the lower levels to which the population flows predominantly quite unambiguously as those listed in Table VI. In most cases the listed combinations have rate constants several orders of magnitude larger than the next possible alternative. Finally the calculated rate constants for the bottlenecks are not too far from the experimental ones with the exception of $d(3)$ and $e(0)$. These two levels are the lowest ones in the d and e states which emit and for them the radiationless relaxation is slowed down so strongly that the radiative decay becomes the rate limiting process (Table IV). Table VI demonstrates also that intersystem crossing back to the singlet states appears as an important relaxation step. This leads as to the last question if the balance of internal conversion and intersystem crossing is in accord with the experiment.

F. The complete relaxation cascade

Up to now the first step in the cascade (Sec. IV D) and the bottlenecks (Sec. IV E) have been discussed. The experiments show that initial population of a high $A\,^1\Pi$ level preserves all lower emitting states with intensities similar to excitation of a lower $A\,^1\Pi$. The cascade touches all lower emitting singlet and triplet levels and this fact has to be re-

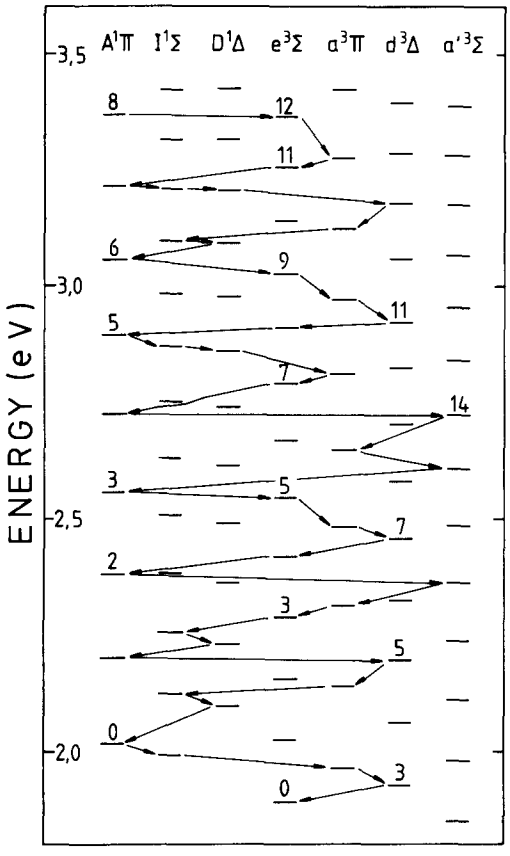

FIG. 10. Outline of the dominant relaxation pathways according to the model presented in the text. The bottlenecks from which emission is observed are indicated by their vibrational numbers.

produced by the model. A bypass of an emitting level in the model would be contradictory to the experiment. The evaluation continues like in Sec. IV E. The rate constants to all neighboring levels are calculated for each intermediate step and the largest ones indicate the relaxation pathway.[33]

The dominant relaxation pathway is shown in Fig. 10 to give an impression. The detailed analysis is cumbersome but the results are summarized quite easily. All radiating levels are reached by the calculated cascade. Triplet levels close enough to the singlet levels are populated to enforce the intersystem crossing back to each $A\ ^1\Pi$ level. Even if pathways are split by comparable rate constants it happens in general that the different pathways are united before a radiating level is reached.

V. CONCLUSION

A detailed relaxation cascade with vibrationally hot emission from several electronic states has been analyzed in terms of mixing of electronic states by intramolecular matrix elements from the gas phase and experimental electron–phonon coupling parameters. The intramolecular spin–orbit coupling matrix elements seem to be sufficiently large to explain the induced radiative triplet–singlet transition rates, the intersystem crossing rate constants, and the internal contrix elements due to the interaction with the matrix. The radiationless rate constants can be treated in the statistical limit because of strong scattering of the coherent superposition of states in the matrix.

The matrix elements have been of the order of 20 cm^{-1}. In NO homogenous interactions with matrix elements in the 1000 cm^{-1} range are known and the model should be applied to discuss the observed energy shifts in rare gas matrices.[13,34] Such large matrix elements should induce relaxation processes with rate constants comparable to phonon relaxation times. A balance of electronic and phonon relaxation processes for interaction of the $A\ ^2\Sigma^+$ Rydberg state with valence states and with the matrix has been reported recently.[13,35] Provided the model gets support on a broader basis it should be possible to explain the influence of different matrices. For CO in Ar and Kr matrices a similar relaxation cascade but with larger rate constants has been established.[33] In the gas phase the increase in rate constants has been attributed to stronger interaction potentials. A larger guest host potential presumably leads to an increase in the electron-phonon coupling constants and thus larger $\langle p'|0\rangle$ terms. Further matrix elements for example by intermolecular spin–orbit interaction can contribute to the mixing for heavier matrices. Also the role of rotational-like scattering processes especially for large gaps should be studied. There is some hope that on this line also systems with more than one internal degree of freedom could be treated quantitatively.

ACKNOWLEDGMENTS

We thank M. Chergui, K. Dressler, H. Schröder, and A. Tramer for stimulating discussions and H. Kühle, U. Fischer, and the staffs of BESSY and DESY for strong experimental backing. This work has been supported by the Bundesministerium für Forschung und Technologie via Contract No. 313 AX 5C 311.

[1]V. E. Bondybey and L. E. Brus, in *Advances in Chemical Physics* edited by I. Prigogine and S. A. Rice (Wiley, New York, 1980), Vol. 41, p. 269.
[2]F. Legay in *Chemical and Biological Applications of Lasers*, edited by C. B. Moore (Academic, New York, 1977), Part II, p. 43.
[3]V. E. Bondybey, Annu. Rev. Phys. Chem. **35**, 591 (1984); A. Amirav, J. Jortner, S. Obojima, and E. C. Lim, Chem. Phys. Lett. **126**, 487 (1986).
[4]H. K. Shin, J. Chem. Phys. **75**, 3821 (1981); L. Young and C. D. Moore, *ibid.* **81**, 3137 (1984); A. Ramsthaler-Sommer, K. E. Eberhardt, and U. Schurath, *ibid.* **85**, 3760 (1986).
[5]V. E. Bondybey and A. Nitzan, Phys. Rev. Lett. **38**, 889, (1977); V. E. Bondybey, J. Chem. Phys. **66**, 995 (1977).
[6]D. Fletcher, Y. Fujimura, and S. H. Lin, Chem. Phys. Lett. **57**, 400 (1978).
[7]G. Jihua, A. Ali, and P. J. Dagdigian, J. Chem. Phys. **85**, 7098 (1986).
[8]J. Goodman and L. E. Brus, J. Chem. Phys. **67**, 4408 (1977).
[9]L. A. Heimbrook, N. Chestnoy, M. Rasaneu, G. P. Schwarz, and V. E. Bondybey, J. Chem. Phys. **83**, 6091 (1985).
[10]S. L. Pan, G. Zumofen, and K. Dressler, J. Chem. Phys. **87**, 3482 (1987).
[11]H. Kühle, J. Bahrdt, R. Fröhling, N. Schwentner, and H. Wilcke, Phys. Rev. B **31**, 4854 (1985); H. Kühle, N. Schwentner, H. Gabriel, and I. Gersonde, Chem. Phys. Lett. **132**, 570 (1986).
[12]G. Zumofen, J. Sedlacek, R. Taubenberger, S. L. Pan, O. Oehler, and K. Dressler, J. Chem. Phys. **81**, 2305 (1984); H. Kühle, R. Fröhling, J.
[14]K. F. Freed and C. Tric, Chem. Phys. **33**, 249 (1978).
[15]H. Lefebvre-Brion and R. W. Field, *Perturbations in the Spectra of Diatomic Molecules* (Academic, New York, 1986).

[16]S. G. Tilford and J. D. Simmons, J. Phys. Chem. Ref. Data **1**, 147 (1972).
[17]R. W. Field, B. G. Wicke, J. D. Simmons, and S. G. Tilford, J. Mol. Spectrosc. **44**, 383 (1972).
[18]M. Lavollée and A. Tramer, Chem. Phys. Lett. **47**, 523 (1977); D. Grimbart, M. Lavollée, A. Nitzan, and A. Tramer, *ibid.* **57**, 45 (1978); M. Lavollée and A. Tramer, Chem. Phys. **45**, 45 (1979); R. W. Field, O. Benoist d'Azy, M. Lavollée, R. Lopez-Delgado, and A. Tramer, J. Chem. Phys. **78**, 2838 (1983).
[19]J. Bahrdt, P. Gurtler, and N. Schwentner, J. Chem. Phys. **86**, 6108 (1987), and references, therein.
[20]P. Gürtler, Thesis, Hamburg, 1979.
[21]E. Boursey (private communication).
[22]H. Wilcke, W. Böhmer, and N. Schwentner, Nucl. Instrum. Methods **204**, 533 (1983).
[23]P. Gürtler, E. Roick, G. Zimmerer, and M. Pouey, Nucl. Instrum. Methods **208**, 835 (1983).
[24]I. Munro and N. Schwentner, Nucl. Instrum. Methods **208**, 59 (1983).
[25]B. Numerov, Publs. Observatoire Central Astrophys. Russ. **2**, 188 (1933).
[26]J. W. Cooley, Math. Comput. **15**, 363 (1961).
[27]J. Fournier, H. H. Mohammed, J. Deson, and C. Vermeil, J. Chem. Phys. **73**, 6039 (1980).
[28]T. C. James, J. Chem. Phys. **55**, 4118 (1971).
[29]P. J. Marcoux, L. G. Piper, and D. W. Setser, J. Chem. Phys. **66**, 351 (1977).
[30]M. Lavollée, Thesis, Paris, 1980.
[31]W. H. Knox, L. F. Mollenauer, and R. L. Forki, in *Ultrafast Phenomena*, edited by G. R. Fleming and A. E. Siegman (Springer, Berlin, 1986), Vol. V, p. 277.
[32]J. Jortner, J. Chem. Phys. **64**, 4860 (1976).
[33]J. Bahrdt, Thesis, Freie Universität Berlin, 1987.
[34]M. Chergui, V. Chandrasekharan, and N. Schwentner (to be published).
[35]M. Chergui, N. Schwentner, and V. Chardrasekharan, J. Lumin. (in press).